An experiment for the precision measurement of the radiative decay mode of the neutron

R.L. Cooper [a,*], C.D. Bass [b], E.J. Beise [c], H. Breuer [c], J. Byrne [d], T.E. Chupp [a], K.J. Coakley [e], M.S. Dewey [b], B.M. Fisher [b], C. Fu [b], T.R. Gentile [b], M. McGonagle [c], H.P. Mumm [b], J.S. Nico [b], A.K. Thompson [b], F.E. Wietfeldt [f]

[a] University of Michigan, Ann Arbor, MI 48109, USA
[b] National Institute of Standards and Technology, Gaithersburg, MD 20899, USA
[c] University of Maryland, College Park, MD 20742, USA
[d] University of Sussex, BN1 9QH, UK
[e] National Institute of Standards and Technology, Boulder, CO 80305, USA
[f] Tulane University, New Orleans, LA 70118, USA

ARTICLE INFO

ABSTRACT

The familiar neutron decay into a proton, electron, and antineutrino can be accompanied by photons with sufficient energy to be detected. We recently reported the first observation of the radiative beta decay branch for the free neutron with photons of energy 15–340 keV. We performed the experiment in the bore of a superconducting magnet where electron, proton, and photon signals were measured. A bar of bismuth germanate scintillating crystal coupled to an avalanche photodiode served as the photon detector that operated in the cryogenic, high magnetic field environment. The branching ratio for this energy region was measured and is consistent with the theoretical calculation. An experiment is under way to measure the branching ratio with an improved precision of 1% relative standard uncertainty and to measure the photon energy spectrum. In this paper, the apparatus modifications to reduce the systematic uncertainties will be described. Central to these improvements is the development of a 12-element detector based on the original photon detector design that will improve the statistical sensitivity. During data acquisition, a detailed calibration program will be performed to improve the systematic uncertainties. The development of these modifications is currently under way, and the second run of the experiment commenced in July 2008.

1. Introduction

The theory of quantum electrodynamics (QED) predicts that a neutron beta decay should be accompanied by photons in the usual final state of a proton, electron, and antineutrino. QED provides a framework to calculate the inner bremsstrahlung (IB) photons that couple to the charged electron and proton [1–4]. The effect of recoil order terms and IB coupling to the weak vertex is included in a calculation that utilizes heavy baryon chiral perturbation theory with explicit Δ degrees of freedom [5,6]. The first run of an experiment to measure the radiative beta decay mode of the free neutron was recently completed at the National Institute of Standards and Technology (NIST) in Gaithersburg, MD [7]. This experiment represents the first observation of this rare decay mode. We measured the branching ratio for neutron decay that is accompanied by photons with energies between 15 and 340 keV to be $(3.13 \pm 0.34) \times 10^{-3}$.

The total uncertainty is the 0.11×10^{-3} statistical uncertainty added in quadrature with the 0.33×10^{-3} systematic uncertainty. This result is in agreement with the theoretical value of 2.85×10^{-3} [8]. This precision is sufficient to check the lowest order theory that considers only electron bremsstrahlung.

In this paper, we describe the motivation and preparation for performing a second, higher precision run of the radiative decay experiment. In Section 2, we describe the overall motivation of this second run. The importance of this experiment as laying the groundwork for future neutron radiative decay experiments is also discussed. In Section 3, we describe the operation of the first run of the experiment. The dominant systematic uncertainties are described since these must be overcome in a new experiment. In Section 4, we describe the upgrades that have been completed or are under way to improve the precision of our measurements.

2. Motivation

A new measurement of the radiative decay mode of the free neutron will improve knowledge about a fundamental

* Corresponding author.
  E-mail address: cooperrl@umich.edu (R.L. Cooper).

semileptonic decay process. Because the neutron decays with low energy and is not subject to nuclear corrections, it is a reliable system to study experimentally and theoretically. Therefore, the effect of QED in this decay is dominated by electron bremsstrahlung. Theoretically, the photon spectrum is dominated by the $1/\omega$ electron bremsstrahlung with vertex contributions occurring linearly in photon energy ω. A precision measurement of the radiative decay mode provides an important test of how QED couples to a weak decay. Furthermore, Low's theorem [9,10] relates the low photon energy QED matrix element for radiative decay to the non-radiative matrix element with no photons in the final state. This means a precise measurement of radiative decay mode in the low photon energy regime can provide information about the parameters that enter in the non-radiative theory.

In the second run of the experiment, we expect to measure the radiative decay branching ratio to a 1% total uncertainty. A new photon detector developed from a similar design to that utilized in the first run will measure the radiative decay for all photons above 15 keV to the endpoint energy of approximately 780 keV. An additional photon detector is being constructed to probe a lower photon energy regime for photon energies from approximately 200 eV to 10 keV. The radiative decay mode will be measured over nearly 4 orders of magnitude in photon energy. In addition, the photon energy spectrum over the proposed energy range will also be measured and compared to theoretical calculations.

This experiment also represents an important exploration to possible future radiative decay experiments below 1% uncertainty. By including all inner bremsstrahlung contributions and retaining recoil order terms, the decay rate differs from the leading electron bremsstrahlung result at $\mathcal{O}(0.5\%)$ [5]. The non-leading-order radiative decay contributions are within reach of a possible next generation experiment, and the development of these new experiments will need to solve many of the problems this experiment must address. By performing the radiative decay experiment with polarized neutrons, new angular correlations arise. The photon momentum is correlated with the polarized neutron's spin, and time-reversal violating correlations could also arise. A measurement of the photon polarization is a test of the $V-A$ structure of the weak current [5]. In all of these possible experiments, the extracted parameters are a result of the 4-body final state of radiative decay versus the 3-body final state in the usual non-radiative beta decay.

3. Overview of the first experiment

An experiment [7,11] was developed to measure high energy photons accompanying the electron, proton, and antineutrino from a neutron beta decay. The experiment was mounted inside the bore of a super-conducting magnet. The bore of the magnet has a 9.5° bend at the upstream end where a silicon surface barrier detector (SBD) was mounted to detect the electrons and protons. The high magnetic field constrains these charged particles to cyclotron orbits as they are guided toward the SBD. The photon detector was located accurately in the main decay region of the bore. It consisted of a 12 mm × 12 mm × 200 mm bar of bismuth germinate (BGO) coupled to an avalanche photodiode (APD). The operation of the photon detector is described in detail elsewhere [12]. An illustration of the radiative decay apparatus is given in Fig. 1.

The prompt electron and delayed proton signals provide a hardware trigger to record all detector waveforms. The presence of a photon is inferred from the analysis of the recorded waveforms. Timing and energy cuts are made in software to extract the final photon spectrum. Radiative decay photons are those photons correlated in time with the electron above the uncorrelated, flat background. Fig. 2 shows an electron–photon
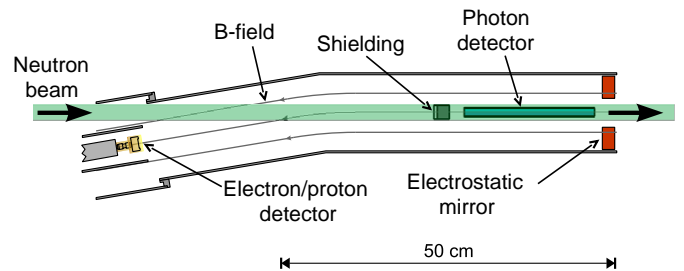

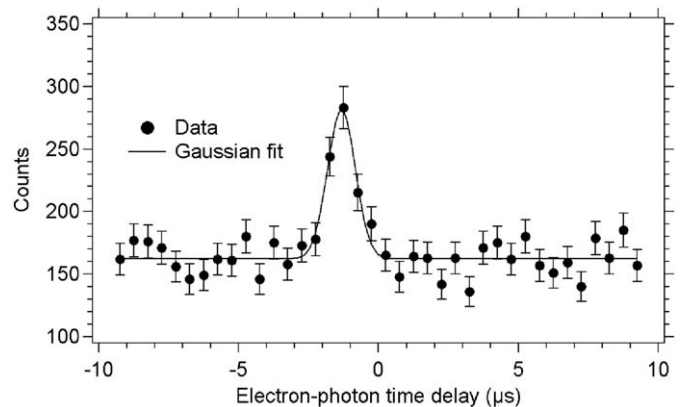**Fig. 1.** Schematic of the radiative decay apparatus.

Fig. 2. Selection of the correlated photons with respect to the electron–photon timing spectrum. The peak represents the correlated event over the uniform, uncorrelated background.

timing spectrum for a particular run. The time delay distribution is not centered about zero due to electronic time delay differences in the SBD and the photon detector channels. The width of the peak is primarily due to photon timing resolution from the photon preamplifier signal. To detect both the electron and the proton in the SBD, the charged particles must be emitted in the same upstream hemisphere with respect to the neutron beam's motion. In order to detect the kinematically preferable case of proton and electron momenta being anti-correlated, an electrostatic mirror was employed in the downstream region of the decay area to reflect the low energy protons. The voltage on the electrostatic mirror is a free parameter of the experiment and provides a means to differentiate neutron radiative decays from background contributions.

Before performing any cuts, the raw photon spectrum was calibrated. The 60 keV gamma ray from ^{241}Am was used as a calibration point for the photon spectrum. Most experimental runs contained two distinct features, a peak at approximately 160 keV and a 511 keV pair-production peak. The peak at 160 keV is the Compton edge associated with the backscattering of gamma rays traveling down the neutron beam line. For the remaining runs, the energy range only contained the backscatter peak. These features were used to monitor the gain of the photon detector. Because the absolute neutron flux was not monitored, the rate of electron–proton–photon events was normalized to the rate of electron–proton events. Without the knowledge of the neutron flux, absolute rates cannot be compared to theory, necessitating a ratio method. A detailed Monte Carlo was used to extract the photon branching ratio from this ratio as a function of electrostatic mirror voltage.

The drift in the photon detector's gain over the duration of the experiment was the largest systematic uncertainty. The photon detector efficiency and response in the bore of the magnet also contribute to the systematic uncertainty. Combined, these

systematic effects contributed 7.5% relative standard uncertainty in the extraction of the branching ratio for photon energies from 15 to 340 keV. The systematic uncertainties will be improved with a more complete calibration procedure for the detectors. There exist other smaller systematic uncertainties that can also be addressed with the hardware improvements described in the next section.
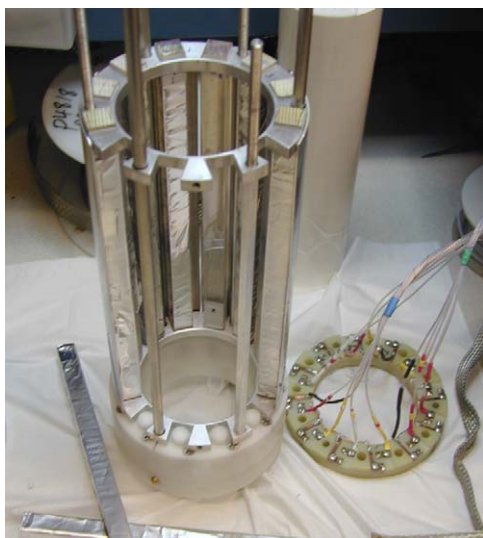
4. Upgrades for second experiment

In order to improve the precision to the goal of 1%, both the statistical and the systematic uncertainties must be lowered. To improve the statistical sensitivity, a larger photon detector is being constructed. This 12-element, coaxial detector will increase the total detection solid angle by a factor of 12. Referring to Fig. 2, additional statistical sensitivity can be achieved by reducing the width of the correlated events peak and reducing the uncorrelated background that must be subtracted. Addressing the systematic concerns will require more frequent calibrations and the dedication of some run time to perform periodic calibrations.

4.1. 12-element detector

A new photon detector with 12 BGO-APD detectors in a coaxial configuration is being developed for use in the second run. The 12 detectors are mounted into a single assembly that can be located accurately (1 mm) in the magnet bore. The 12 APDs are mounted on a G10-FR4 fiberglass mount and pressed against the open ends of the BGO with a nylon, spring-loaded mount. The entire system is assembled on stainless steel struts and aluminum rings hold the BGOs in a precise position. Mounted upstream of the photon detector is a lead–copper design shield to reduce the total uncorrelated background events from the reactor. The shield is situated such that it occludes some of the photon detector elements from the correlated backgrounds from the SBD. Mounted downstream is an aluminum embedded cup that serves as the electrostatic mirror. The outer cup is grounded and shields any stray electrostatic fields from the APDs or supply wires. A photograph of the assembled 12-element detector with the electrostatic mirror removed for clarity is shown in Fig. 3.

Because each APD has a unique breakdown voltage, a high voltage power supply that can be set individually for each channel

Fig. 3. A photograph of the 12-element detector with BGO crystals mounted in the assembly on the left and APDs on the right.

is used to optimize the signal-to-noise for each detector. This optimal operating voltage is typically 25 V below the breakdown voltage which is approximately 1400 V when the APD is near 77 K. The APD breakdown voltage and thus the gain are very sensitive to the temperature, and to minimize temperature drift, the detector assembly is coupled to the liquid nitrogen jacket of the superconducting magnet.

To address the systematic uncertainties associated with the detector response, a series of vacuum compatible gamma-ray sources can be inserted into the operating detector to test the response of the point sources. The response of the detector includes detection of photons that Compton scatter off of the mounting and shielding equipment and back to the detector. Spatial dependence can be checked in these tests as well. The detector response is being modeled by MCNP5 [13] and Geant4 [14,15] Monte Carlo packages.

The statistical uncertainty should be reduced below 1% because of several improvements. First, the increased solid angle for detection will give 12 times the total photon events detected. The addition of a larger lead–copper shield is intended to reduce the uncorrelated photon background that is subtracted from the correlated photon peak. During the first run, an 8-bit, bipolar oscilloscope card was used to digitize all the waveform data collected. A 14-bit, bipolar oscilloscope card will replace the original card, and it will reduce the digitization noise which contributes to the width of the correlated photon peak.

4.2. APD direct detection

Large area APDs can be used to directly detect radiation below the threshold of the scintillator-APD detector. Bremsstrahlung is known to vary as $1/\omega$ where ω is the photon energy, and the APD will see a higher photon rate per unit area and per unit energy. In our tests, we have observed a noise threshold of 200 eV or less for photons directly detected by the APDs. Photons above 5 keV are detected with reduced efficiency because they do not deposit all of their energy in the device. Direct detection does not suffer from the slow rise time associated with BGO; in a brief test during the experiment, we observed a much narrower width and better signal-to-noise than the timing curve in Fig. 2. The disadvantage of direct detection is that it provides a smaller solid angle for the same cost.

A new array of four large area APDs (28 mm × 28 mm) is being assembled in a coaxial configuration. In the next experimental run, this direct detection assembly will be located between the lead–copper shield and the 12-element detector. By running both detector arrays simultaneously, some information can be gleaned about photon angular correlations. Offline tests in a cryostat with 5.9 keV X-rays from a ^{55}Fe source have been performed on a single bare APD. In addition, X-ray fluorescence can be used to test the lower energy response of the APD [16]. A sample of $CaSO_4$ was located in the vacuum of the cryostat in line of sight to the APD and illuminated by the ^{55}Fe source through a thin plastic window. Fig. 4 shows the response of the APD for iron (5.9 keV), calcium (3.69 keV), sulfur (2.31 keV), as well as aluminum (1.49 keV) from the apparatus itself.

4.3. Absolute decay rate measurements

In the first run, the branching ratio was extracted from the ratio of the electron–proton–photon events to the electron–proton (no observed photon) events as a function of electrostatic mirror voltage. This procedure was necessary because there was no way to calibrate the observed detection rates absolutely. For the second run, a neutron flux monitor will be mounted downstream
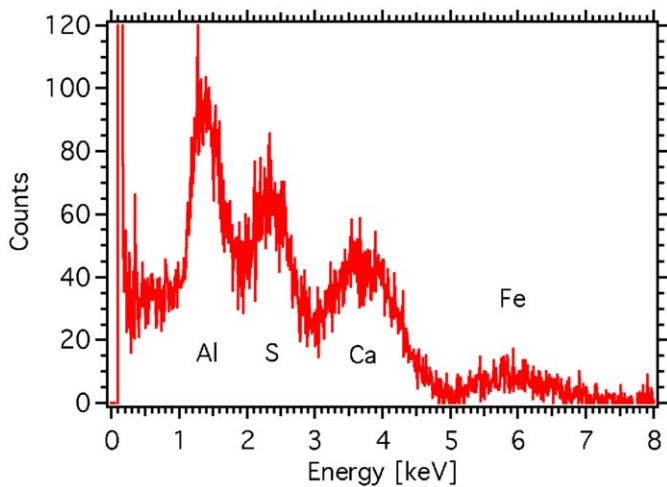
Fig. 4. X-ray fluorescence spectrum from CaSO$_4$ irradiated by a 5.9 keV iron X-ray.

Fig. 5. Calibration source spectra for ^{137}Cs (662 keV) and ^{133}Ba with ^{241}Am (60 keV) overlaid for comparison. The main ^{133}Ba gamma rays are at 80, 303, and 356 keV.

of the experimental apparatus; it will operate by counting the reaction products from a neutron capture on a ^{6}Li deposit. This neutron flux detector measures the $1/v$ weighted neutron flux where v is the neutron velocity. This provides a measure of the total neutron density in the polychromatic neutron beam.

Since the branching ratio for high energy photon production is relatively small, most of the events will be electron–proton events with no correlated photon. In the first run, over 10^7 events were without a photon. The differential decay rate for unit electron energy dE_e, solid angle dΩ_e, and unit antineutrino solid angle dΩ_v for these non-radiative decays is [17]

$$\frac{d\Gamma}{dE_e\, d\Omega_e\, d\Omega_v} \propto |\mathbf{p}_e| E_e (E_0 - E_e)^2 \left(1 + a\frac{\mathbf{p}_e \cdot \mathbf{p}_v}{E_e E_v}\right) \qquad (1)$$

where E_0 is the maximum electron energy and $a = (1 - \lambda^2)/(1 + 3\lambda^2)$ in the Standard Model. The parameter λ is the ratio of the weak interaction's axial vector coupling to its vector coupling. Experiments that measure the proton energy spectrum can measure a. An experiment has already used this method in a Penning trap to measure a [18], and another is currently operating [19]. The electrostatic mirror is effectively a proton spectrometer that is sensitive to the longitudinal momentum component. While this reduces its sensitivity as a proton energy spectrometer, the electron–proton decay rate as a function of voltage can be benchmarked with Monte Carlo given the known value of a.

4.4. Calibration routine

Thorough testing is under way to characterize the detector's response to gamma-ray sources. These tests have been performed at both room and cryogenic operating temperatures. At cryogenic temperatures, tests were also performed with and without the 4.6 T magnetic field. The stability of the noise and gain of the detector over long periods of operation, including over cryogen fill cycles, has been documented.

During the experimental run, calibration runs to record the photon singles will be carried out. No photon singles measurements were performed during the first experiment. Instead, all photons which arrived in a 50 μs sampling window around an electron–proton trigger were summed. This resulted in poor statistical sensitivity to the calibration features. The observed photon singles rate in the first experiment was approximately 100 s^{-1} per detector, and this should be lower (but still usable as a calibration) in the next experiment. By utilizing a variety of

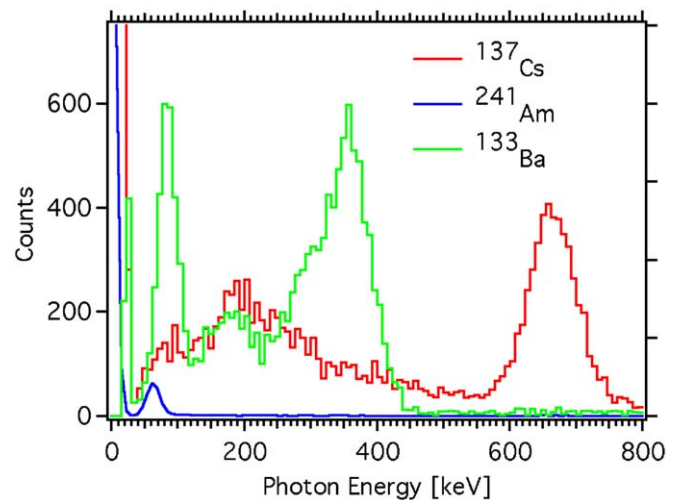spectra features (511 keV, bismuth X-ray, backscatter peak, etc.) and external sources, a calibration in photon singles will quickly achieve the statistical sensitivity needed to improve the 7.5% systematic uncertainty in the photon detector from the first run.

By combining the improved calibrations and offline tests, other systematic uncertainties can be improved. The photon detector efficiency and resolution each require a correction and have a systematic uncertainty associated with these corrections. This will be important for both the branching ratio and the photon energy spectrum. Calibration tests with gamma-ray sources have been completed at cryogenic temperatures in a test cryostat. Fig. 5 shows the measured gamma-ray spectra from ^{137}Cs (662 keV) and ^{133}Ba (predominantly 80, 303, and 356 keV) with that from ^{241}Am (60 keV) overlaid for comparison.

5. Summary

An experiment has been completed in which the radiative decay mode of the free neutron was observed for the first time. We measured the branching ratio for neutron decay accompanied by photons with energy from 15 to 340 keV to be $(3.13 \pm 0.34) \times 10^{-3}$. The 11% total uncertainty is the addition of the 0.11×10^{-3} statistical uncertainty with the 0.33×10^{-3} systematic uncertainty in quadrature.

The second run of the experiment began in the summer of 2008 at the NG-6 cold neutron beamline at NIST Center for Neutron Research. The experiment will operate for approximately one year which should be sufficient for achieving adequate statistical sensitivity and allowing time to thoroughly investigate all of the systematic uncertainties to 1% relative standard uncertainty.

References

[1] F. Glück, Phys. Rev. D 47 (1993) 2840.
[2] Y.V. Gaponov, R.U. Khafizov, Phys. Atom. Nucl. 59 (1996) 1213.
[3] Y.V. Gaponov, R.U. Khafizov, Phys. Lett. B 379 (1996) 7.
[4] Y.V. Gaponov, R.U. Khafizov, Nucl. Instr. and Meth. A 440 (2000) 557.
[5] V. Bernard, S. Gardner, U.-G. Meißner, C. Zhang, Phys. Lett. B 593 (2004) 105.
[6] V. Bernard, S. Gardner, U.-G. Meißner, C. Zhang, Phys. Lett. B 599 (2004) 348.
[7] J.S. Nico, et al., Nature 444 (2006) 1059.
[8] S. Gardner, Private communication, 2006.
[9] F.E. Low, Phys. Rev. 110 (1958) 974.
[10] S.L. Adler, Y. Dothan, Phys. Rev. 151 (1966) 1267.

[11] R.L. Cooper, The radiative decay mode of the free neutron, Ph.D. Thesis, University of Michigan, 2008.

[12] T.R. Gentile, et al., Nucl. Instr. and Meth. A 579 (2007) 447.

[13] F.B. Brown, et al., A General Monte Carlo N-Particle Transport Code, Version 5 LA-UR-03-1987, 2003.

[14] S. Agostinelli, et al., Nucl. Instr. and Meth. A 506 (2003) 250.

[15] J. Allison, et al., IEEE Trans. Nucl. Sci. NS-53 (2006) 270.

[16] L. Fernandes, et al., X-ray Spectrom. 30 (2001) 164.

[17] J.D. Jackson, S.B. Treiman, H.W. Wyld Jr., Phys. Rev. 106 (1957) 517.

[18] J. Byrne, et al., J. Phys. G Nucl. Part. Phys. 28 (2002) 1325.

[19] F. Glück, et al., Eur. Phys. J. A 23 (2005) 135.